# Inorganic Chemistry

including bioinorganic chemistry

March 18, 2013
Volume 52, Number 6
pubs.acs.org/IC


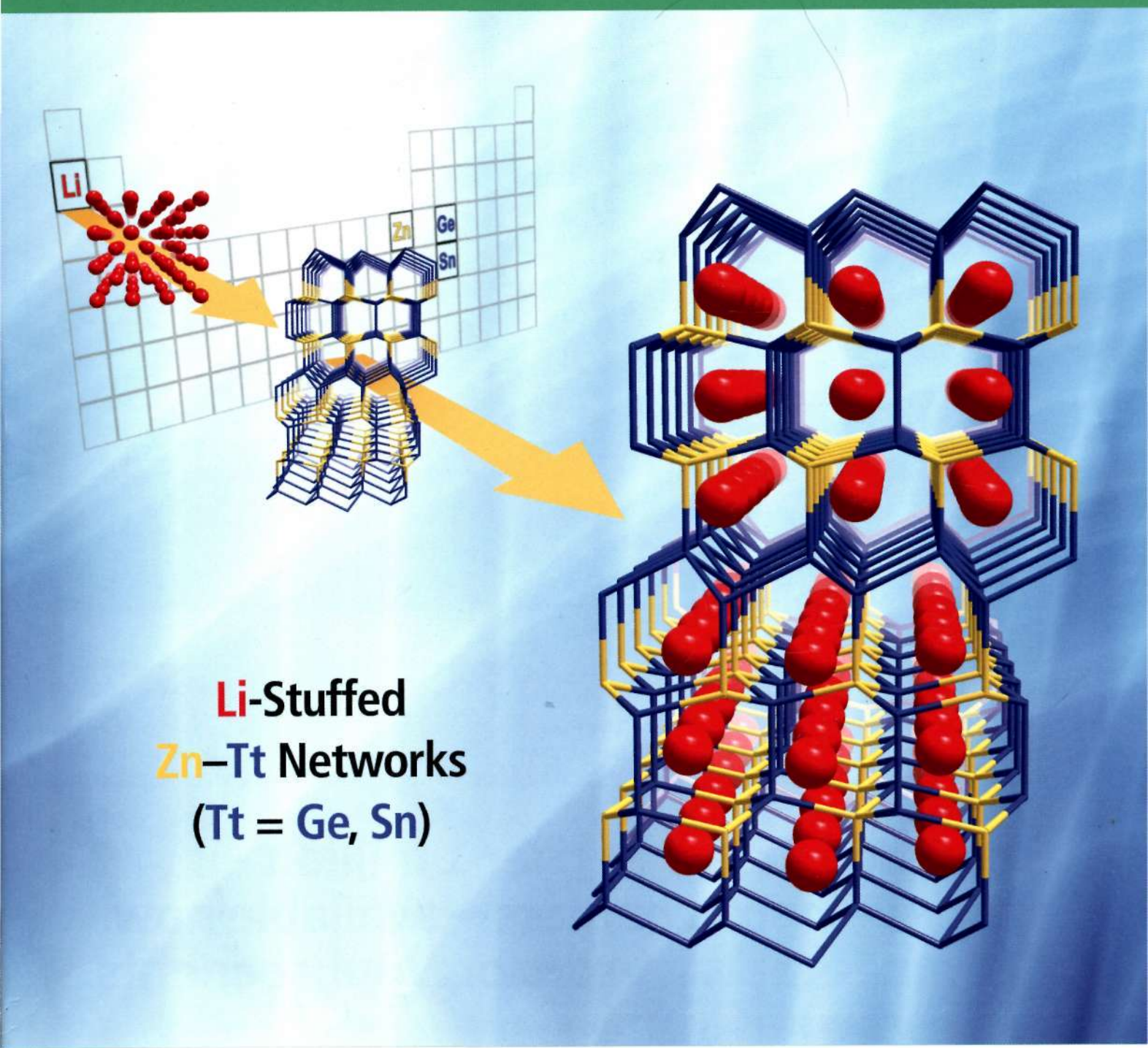


## Li-Stuffed Zn–Tt Networks (Tt = Ge, Sn)


ACS Publications
MOST TRUSTED. MOST CITED. MOST READ.

www.acs.org

Inorganic Chemistry

MARCH 18, 2013
VOLUME 52 ISSUE 6

INOCAJ 52(6) 2787–3404 (2013)
ISSN 0020-1669


**ON THE COVER:** Ternary Li–Zn–Tt (Tt = Ge, Sn) phases with Li-stuffed diamond polytype like Zn–Tt network structures are obtained by the reaction of Li with Zn and Ge or Sn. See S. Stegmaier and T. F. Fässler, p 2809.

## Communications



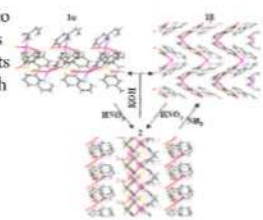



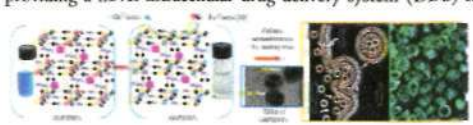

# Articles

2817 dx.doi.org/10.1021/ic301579g

**Manganese-Based Layered Coordination Polymer: Synthesis, Structural Characterization, Magnetic Property, and Electrochemical Performance in Lithium-Ion Batteries**

Qi Liu,* Lili Yu, Ying Wang, Yunzhou Ji, Josip Horvat, Mei-Ling Cheng, Xiaoyan Jia, and Guoxiu Wang*

Manganese-based layered coordination polymer ($[Mn(tfbdc)(4,4'\text{-bpy})(H_2O)_2]$, Mn−LCP) with microporous structure was synthesized by reaction of 2,3,5,6-tetrafluoroterephthalatic acid($H_2$tfbdc) and 4,4′-bipyridine(4,4′-bpy) with manganese(II) acetate tetrahydrate in water solution. Mn−LCP was characterized by elemental analysis, IR spectra, thermogravimetric analysis, X-ray single-crystal structure analysis, and powder X-ray diffraction.

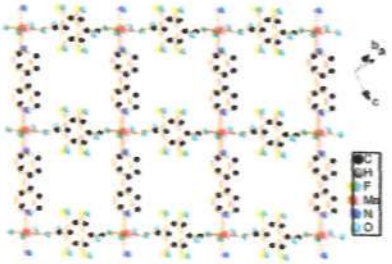


2823 dx.doi.org/10.1021/ic301598n

**Expanded Porous MOF-505 Analogue Exhibiting Large Hydrogen Storage Capacity and Selective Carbon Dioxide Adsorption**

Baishu Zheng,* Ruirui Yun, Junfeng Bai,* Zhiyong Lu, Liting Du, and Yizhi Li

An expanded NbO-type copper metal−organic framework (NJU-Bai12) has been successfully constructed from a nanosized rectangular alkyne-bridging tetracarboxylate ligand and copper(II) paddlewheel secondary building unit, exhibiting large hydrogen storage capacity and selective carbon dioxide adsorption.

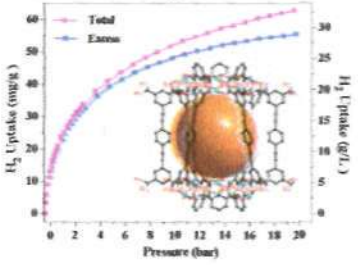


2830 dx.doi.org/10.1021/ic301660e

**X-ray Absorption Spectroscopy of a Quantitatively Mo(V) Dimethyl Sulfoxide Reductase Species**

M. Jake Pushie, Julien J. H. Cotelesage, Ganna Lyashenko, Russ Hille, and Graham N. George*

X-ray absorption spectroscopy of an extensively studied Mo(V) form of *Rhodobacter sphaeroides* dimethylsulfoxide reductase (the high-g split species) shows that previously suggested structures for the active site are likely incorrect.

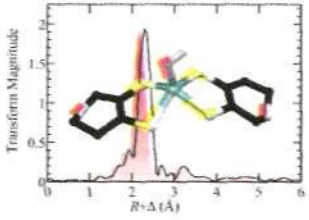




2838 dx.doi.org/10.1021/ic301657c

**Molecules with High Bond Orders and Ultrashort Bond Lengths: CrU, MoU, and WU**

Fernando Ruipérez, Gabriel Merino, Jesus M. Ugalde, and Ivan Infante*

The effective bond order of the MoU dimer (5.5) is higher than that of the tungsten dimer (5.2), known to date as the molecule with the highest bond order in the whole periodic table. The MU (M = Cr, Mo, W) heterodimers present also ultrashort bond distances and remarkably large dissociation energies.

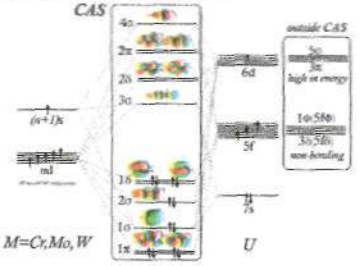


2844 dx.doi.org/10.1021/ic301733r

**Unexpected Electronic Process of $H_2$ Activation by a New Nickel Borane Complex: Comparison with the Usual Homolytic and Heterolytic Activations**

Guixiang Zeng and Shigeyoshi Sakaki*

The H−H $\sigma$-bond was cleaved under the cooperation of the electron-rich nickel center and the electron-deficient borane to form an unprecedented hydridoborohydrido complex through a four-center transition state. The electronic process is different from those of the usual homolytic and heterolytic $H_2$ activation reactions.

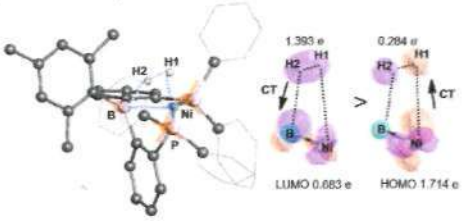


2854 dx.doi.org/10.1021/ic301795j

**γ-Cyclodextrin Cuprate Sandwich-Type Complexes**

Abdulaziz A. Bagabas,* Marco Frasconi, Julien Iehl, Brad Hauser, Omar K. Farha, Joseph T. Hupp, Karel J. Hartlieb, Youssry Y. Botros, and J. Fraser Stoddart*

Sandwich-type complexes based on γ-cyclodextrin (orange) and $Cu^{2+}$ (purple) ions, with alkali-metal (blue) ions ($Li^+$, $Na^+$, and $Rb^+$), have been prepared and characterized structurally by single-crystal X-ray diffraction, with the identity of the alkali-metal ion strongly influencing the precise nature of the solid-state structures. Gas uptake studies reveal promising $CO_2$ sorption properties, particularly for the $Cu^{2+}/Rb^+$ complex.

2862 Ⓢ dx.doi.org/10.1021/ic301936k

**Tuning the Structure and Magnetism of Heterometallic Sodium(1+)–Cobalt(2+) Formate Coordination Polymers by Varying the Metal Ratio and Solvents**

Jiong-Peng Zhao, Song-De Han, Ran Zhao, Qian Yang, Ze Chang, and Xian-He Bu*

Through variation of the metal ratio and solvents, the structure and magnetism of three new heterometallic sodium(1+)–cobalt(2+) formate coordination polymers with different ratios of $Co^{2+}$ and $Na^{+}$ ions have been well tuned.

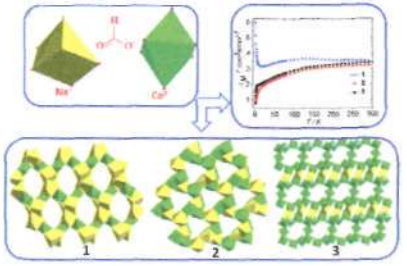


2870 Ⓢ dx.doi.org/10.1021/ic302483e

**Azo Complexes of Osmium(II): Preparation and Reactivity of Organic Azide and Hydrazine Derivatives**

Gabriele Albertin,* Stefano Antoniutti, Laura Bonaldo, Alessandra Botter, and Jesús Castro

The preparation of unprecedented organic azide complexes of osmium $[OsCl(\eta^1\text{-}N_3R)(CO)(PPh_3)_2L]BPh_4$ is described. The reaction of the benzylazide derivative leading to the N-protio imine complex $[OsCl(CO)\{\eta^1\text{-}NH{=}C(H)C_6H_4\text{-}4\text{-}CH_3\}(PPh_3)_2\{P(OEt)_3\}]BPh_4$ is also reported. Mixed-ligand hydrazine and aryldiazene complexes of the types $[OsCl(CO)(RNHNH_2)(PPh_3)_2L]BPh_4$ and $[OsCl(CO)(ArN{=}NH)(PPh_3)_2L]BPh_4$ were also prepared.

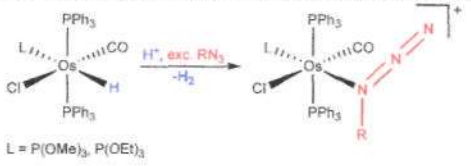


2880 Ⓢ dx.doi.org/10.1021/ic302099y

**Synthesis, Structure, Spectroscopic Characterization, and Protein Binding Affinity of New Water-Soluble Hetero- and Homometallic Tetranuclear $[Cu^{II}_2Zn^{II}_2]$ and $[Cu^{II}_4]$ Clusters**

Ayan Patra, Tamal K. Sen, Atanu Ghorai, Ghezai T. Musie,* Swadhin K. Mandal, Utpal Ghosh, and Manindranath Bera*

Two new water-soluble hetero- and homometallic tetranuclear clusters, $Na_4[Cu_2Zn_2(ccdp)_2(\mu\text{-}OH)_2]\cdot CH_3OH\cdot 6H_2O$ (**1**) and $K_3[Cu_4(ccdp)_2(\mu\text{-}OH)(\mu\text{-}OH_2)]\cdot 14H_2O$ (**2**), have been synthesized and characterized by exploiting the flexibility, chelating ability, and bridging potential of a carboxylate-rich dinucleating ligand. These clusters are investigated for their binding affinity with the protein bovine serum albumin in an aqueous medium at physiological pH using fluorescence spectroscopy.

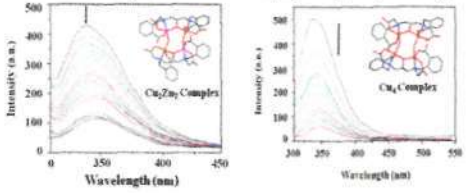




2891 Ⓢ dx.doi.org/10.1021/ic3021113

**Influence of Halogen Bonding Interaction on Supramolecular Assembly of Coordination Compounds; Head-to-Tail N···X Synthon Repetitivity**

Hamid Reza Khavasi* and Alireza Azhdari Tehrani

One of the common features in the crystal structures of these complexes is that there is a strong tendency to form halogen bonding synthons. The second common feature of crystal structures of complexes studied here, is the selectivity of metal ion coordination site.

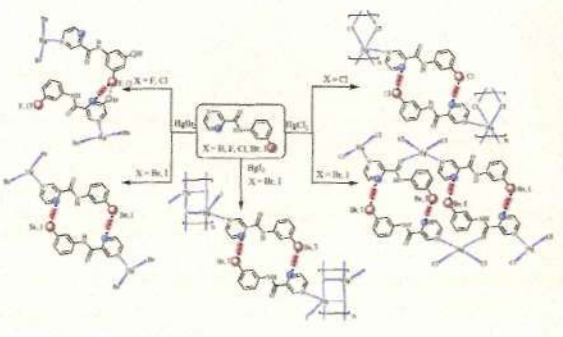

2906 Ⓢ dx.doi.org/10.1021/ic302173g

**Communication between Remote Moieties in Linear Ru–Ru–Ru Trimetallic Cyanide-Bridged Complexes**

German E. Pieslinger, Pablo Albores, Leonardo D. Slep, Benjamin J. Coe, Cliff J. Timpson, and Luis M. Baraldo*

The mixed-valence complexes *trans*-$[Ru(L)_4\{(\mu\text{-}CN)Ru(py)_4Cl\}_2]^{3+}$ (L = pyridine or 4-methoxypyridine) show an intense transition assignable to a charge transfer between the remote ruthenium units. This is more intense when L = 4-methoxypyridine, which gives evidence of the role of the bridging ruthenium unit in promoting mixing between the $d\pi$ orbitals of the terminal fragments.

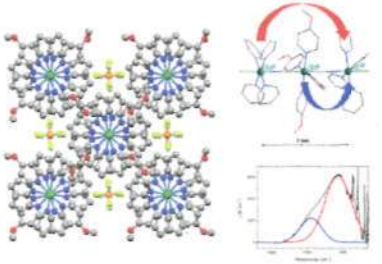

2918 S dx.doi.org/10.1021/ic302222q

**p-Carborane-Bridged Bipyridine Ligands for Energy Transfer between Two Iridium Centers**

M. Teresa Indelli,* Thomas Bura, and Raymond Ziessel*

Two disparate Ir(III) complexes displaying different optical properties were linked via ethynyl-bipyridine ligands to a closo-*para*-carborane spacer. The electronic levels the Ir chromophores were modulated by changing the peripherical ligand from 2′,4′-difluoro-2-phenylpyridine to dibenzo[*a*,*c*]phenazine. Slow energy transfer is occurring between both Ir(III) subunits due to the absence of extensive electronic delocalization.

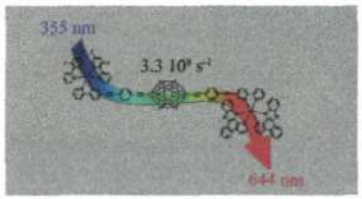


2927 S dx.doi.org/10.1021/ic302611a

**Decarbonylative Halogenation by a Vanadium Complex**

Sujoy Rana, Rameezul Haque, Ganji Santosh, and Debabrata Maiti*

The first metal-mediated decarbonylative halogenation reaction starting from the divanadium oxoperoxo complex $K_3V^{5+}{}_2(O_2{}^{2-})_4(O^{2-})_2(\mu\text{-OH})$ has been reported. A *concerted* decarbonylative halogenation reaction is proposed based on experimental observations.

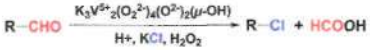


2933 S dx.doi.org/10.1021/ic302327p

**Preparation of Primary Amine Derivatives of the Magic-Size Nanocluster $(CdSe)_{13}$**

Yuanyuan Wang, Yi-Hsin Liu, Ying Zhang, Paul J. Kowalski, Henry W. Rohrs, and William E. Buhro*

Compounds $[(CdSe)_{13}(RNH_2)_{13}]$ (R = *n*-propyl, *n*-pentyl, *n*-octyl, and oleyl) are conveniently prepared by a common amine-bilayer-template synthesis and exhibit a common stoichiometry. These are the first derivatives of magic-size CdSe nanoclusters to be isolated in purity. Analysis of low-angle XRD data provides an experimental estimate of the diameter of the $(CdSe)_{13}$ nanocluster at 0.8 nm, which matches theory. $[(CdSe)_{13}(n\text{-propylamine})_{13}]$ is obtained as a yellowish-white solid in gram quantities.

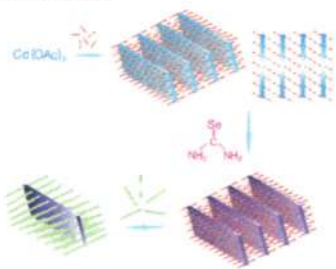




2939 S dx.doi.org/10.1021/ic302330u

**pH-Controlled Coordination Mode Rearrangements of "Clickable" Huisgen-Based Multidentate Ligands with $[M^I(CO)_3]^+$ (M = Re, $^{99m}$Tc)**

Shalina C. Bottorff, Adam L. Moore, Ariana R. Wemple, Dejan-Krešimir Bučar, Leonard R. MacGillivray, and Paul D. Benny*

An alkyne-functionalized 2-[(pyridin-2-ylmethyl)amino]acetic acid (PMAA) ligand was investigated using two strategies (*click, then chelate* and *chelate, then click*) with *fac*-$[M^I(OH_2)_3(CO)_3]^+$ (M = Re, $^{99m}$Tc) and the $Cu^I$-catalyzed Huisgen click reaction to determine the influence of assembly on the coordination species observed. Of three possibilities, two coordination modes were observed in the reaction based on solution pH, which could reversibly intraconvert upon addition of acid ($N_{tri}N_{amine}N_{py}$) or base ($O,N_{amine}N_{py}$). Coordination mode rearrangement was studied on the macroscopic Re and radiotracer $^{99m}$Tc level.

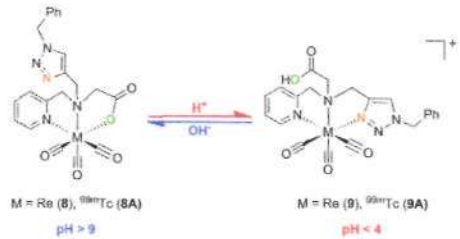


2951 S dx.doi.org/10.1021/ic302334x

**Solvent-Induced Structural Dynamics in Noninterpenetrating Porous Coordination Polymeric Networks**

Raghavender Medishetty, Daram Jung, Xiaokai Song, Dongwook Kim, Shim Sung Lee,* Myoung Soo Lah,* and Jagadese J. Vittal*

Flexible MOFs have been synthesized, and in Zn-MOF solvent, molecules reversibly exchange with four different solvents via SCSC manner suggesting dynamic nature of framework, whereas the Cd-MOF shows selective adsorption of $CO_2$ over other gases.

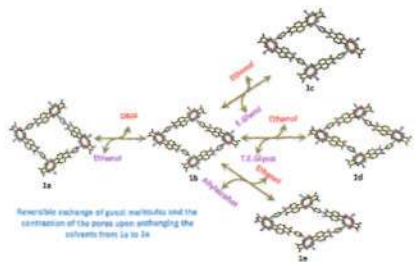

3007 dx.doi.org/10.1021/ic3024666

**Tunable Color of $Ce^{3+}/Tb^{3+}/Mn^{2+}$-Coactivated $CaScAlSiO_6$ via Energy Transfer: A Single-Component Red/White-Emitting Phosphor**

Wei Lü, Ning Guo, Yongchao Jia, Qi Zhao, Wenzhen Lv, Mengmeng Jiao, Baiqi Shao, and Hongpeng You*

Novel tunable red/white-emitting $CaScAlSiO_6:Ce^{3+},Tb^{3+},Mn^{2+}$ phosphors have been synthesized for UV-pumped light-emitting diodes. White light can be achieved by combining the four emission colors (a blue band of 380 nm, a green band of 542 nm, a yellow band of 574 nm, and a red band of 670 nm) in this system.

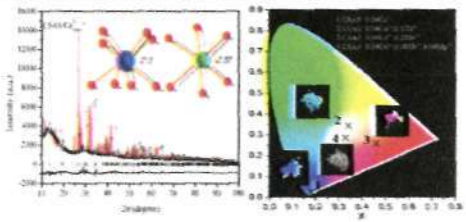

3013 dx.doi.org/10.1021/ic3024716

**Magnetic Ordering in Tetragonal 3d Metal Arsenides $M_2As$ (M = Cr, Mn, Fe): An Ab Initio Investigation**

Yuemei Zhang, Jakoah Brgoch, and Gordon J. Miller*

The electronic and magnetic structures of the tetragonal 3d metal arsenides, $Cr_2As$, $Mn_2As$, and $Fe_2As$, were examined on the basis of density functional calculations to identify chemical influences on their respective patterns of antiferromagnetically (AFM) ordered local moments at the 3d metal sites. Moreover, a magnetostrictive tetragonal-to-orthorhombic distortion was predicted to occur in $Cr_2As$.

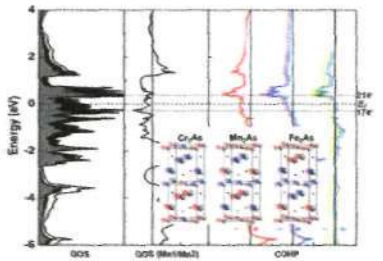


3022 dx.doi.org/10.1021/ic302473j

**Synthesis, Structure, and Reactivity of an Anionic Zr–Oxo Relevant to $CO_2$ Reduction by a Zr/Co Heterobimetallic Complex**

Jeremy P. Krogman, Mark W. Bezpalko, Bruce M. Foxman, and Christine M. Thomas*

Synthesis and structural parameters of a $CO_2$-derived Zr–oxo anion is described in the context of a hypothetical $CO_2$ reduction scheme. This anionic oxo species reacts readily with electrophiles and also reversibly reacts with $CO_2$ to generate a Zr-bound carbonate species.

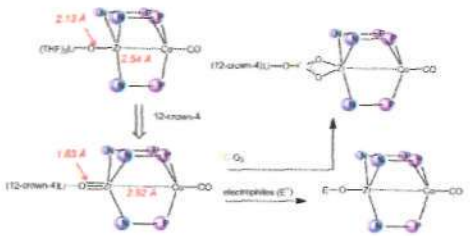




3032 dx.doi.org/10.1021/ic302485c

**Oxo–Mo(IV)(dithiolene)thiolato Complexes: Analogue of Reduced Sulfite Oxidase**

Joyee Mitra and Sabyasachi Sarkar*

Sulfite oxidase on reduction to the $Mo^{IV}$ state retains the minimum structural feature $[Mo^{IV}O(S–S)(SR)]^-$ (with S–S = ene–dithiolene, SR = Scys) moiety that responds to two sequential one-electron oxidations at low potential via an EPR-active intermediate $Mo^{V}$ species. The role of redox-active dithiolene as an electron transfer gate between the molybdenum center and the external oxidants has been shown here. The transient sulfur-based radical generated at the initial oxidation phase is monitored by EPR, which has been supported by DFT calculation, showing a ligand-based SOMO. The bite angle of the stabilizing ligand and dihedral angle of thiolato controls the nature of the SOMO. This is relevant to protein breathing with the change in the oxidation state of the molybdenum active site.

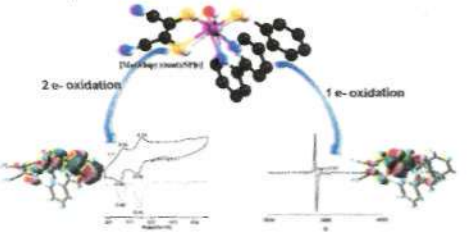


3043 dx.doi.org/10.1021/ic3024953

**Low Oxidation State Iron(0), Iron(I), and Ruthenium(0) Dinitrogen Complexes with a Very Bulky Neutral Phosphine Ligand**

Ryan Gilbert-Wilson, Leslie D. Field,* Stephen B. Colbran, and Mohan M. Bhadbhade

A series of dinitrogen complexes have been synthesized on Ru and Fe containing the tripodal phosphine ligand $P^2P_3^{Cy}$. These include the Ru(0), Fe(0), and Fe(I) dinitrogen complexes. The first Ru(I) chloro complex was also synthesized and characterized. Protonation of the Ru(0) and Fe(0) dinitrogen complexes gave the Ru(II) and Fe(II) hydrido dinitrogen complexes.

3054 dx.doi.org/10.1021/ic302513c

**Stable Plumbylene Dichalcogenolate Monomers with Large Differences in Their Interligand Angles and the Synthesis and Characterization of a Monothiolato Pb(II) Bromide and Lithium Trithiolato Plumbate**

Brian D. Rekken, Thomas M. Brown, Marilyn M. Olmstead, James C. Fettinger, and Philip P. Power*

The plumbylenes, $Pb(ChAr^{Ph_6})_2$ (Ch = O (**1**), S (**2**); $Ar^{Ph_6} = C_6H_3$-2,6-$(C_6H_3$-2,6-$Pr^i_2)_2$) are the first fully characterized monomeric, two-coordinate, lead dichalcogenolates in the solid state. They were synthesized by alcoholysis and salt metathesis routes. Structural studies showed that the acute S–Pb–S angle (ca. 77.2°) is significantly narrower than the corresponding O–Pb–O angle (ca. 99.9°). Based on the $^{207}Pb$ NMR and electronic spectroscopy, the HOMO–LUMO energy separation is shown to decrease from the bisaryloxo plumbylene to the bisthiolato derivative.

3063 dx.doi.org/10.1021/ic3025342

**Synthesis, Lanthanide Coordination Chemistry, and Liquid–Liquid Extraction Performance of CMPO-Decorated Pyridine and Pyridine *N*-Oxide Platforms**

Daniel Rosario-Amorin, Sabrina Ouizem, Diane A. Dickie, Yufeng Wen, Robert T. Paine,* Jian Gao, John K. Grey, Ana de Bettencourt-Dias, Benjamin P. Hay, and Lætitia H. Delmau

Syntheses for four hybrid CMPO decorated pyridine *N*-oxide ligands and selected coordination chemistry with lanthanide cations as well as liquid–liquid extraction analyses for the ligands are described.

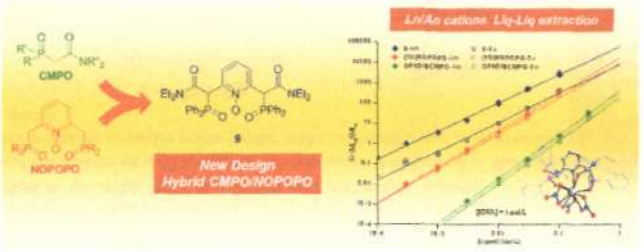


3084 dx.doi.org/10.1021/ic302499f

**Copper(II) Complexes of Tetradentate Pyridyl Ligands Supported on Keggin Polyoxometalates: Single-Crystal to Single-*Crystal Transformations Promoted by Reversible Dehydration Processes***

Amaia Iturrospe, Beñat Artetxe, Santiago Reinoso, Leire San Felices, Pablo Vitoria, Luis Lezama, and Juan M. Gutiérrez-Zorrilla*

Single-crystal to single-crystal transformations promoted by reversible dehydration processes have been studied for two new hybrid compounds constructed from Keggin type polyoxometalates and copper(*II*) complexes of tetradentate ligands containing amine and pyridyl groups, $[Cu(bpmen)(H_2O)][SiW_{12}O_{40}\{Cu(bpmen)\}]$ (**1**) and $[SiW_{12}O_{40}\{Cu(bpmpn)(H_2O)\}_2]\cdot 3H_2O$ (**2**). Structural transformations to the high-temperature, crystalline **1a** and **2a** anhydrous phases have been followed by both powder and single-crystal X-ray diffraction.

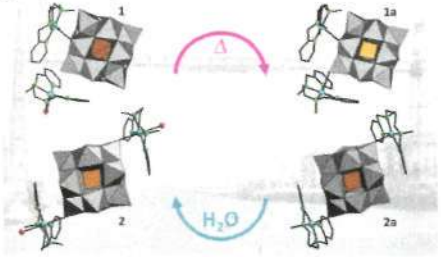




3094 dx.doi.org/10.1021/ic302573x

**Effects of Proton Acceptors on Formation of a Non-Heme Iron(IV)–Oxo Complex via Proton-Coupled Electron Transfer**

Yusuke Nishida, Yuma Morimoto, Yong-Min Lee, Wonwoo Nam,* and Shunichi Fukuzumi*

Rates of formation of a non-heme iron(IV)–oxo complex, $[Fe^{IV}(O)(N4Py)]^{2+}$, via electron-transfer oxidation of $[Fe^{III}(OH)(N4Py)]^{2+}$ in acetonitrile containing $H_2O$ were accelerated as much as 390-fold by addition of proton acceptors. The one-electron oxidation potential of $[Fe^{III}(OH)(N4Py)]^{2+}$ was shifted by −0.28 V in the presence of $TsO^-$ (10 mM). The electron-transfer oxidation occurred following the deprotonation equilibrium with proton acceptors in which deuterium kinetic isotope effects were observed when $H_2O$ was replaced by $D_2O$.

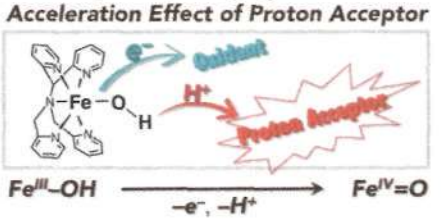


3102 dx.doi.org/10.1021/ic3025759

**Luminescence and Energy Transfer Properties of $Ca_2Ba_3(PO_4)_3Cl$ and $Ca_2Ba_3(PO_4)_3Cl$:A (A = $Eu^{2+}$/$Ce^{3+}$/$Dy^{3+}$/$Tb^{3+}$) under UV and Low-Voltage Electron Beam Excitation**

Mengmeng Shang, Dongling Geng, Dongmei Yang, Xiaojiao Kang, Yang Zhang, and Jun Lin*

$Ca_2Ba_3(PO_4)_3Cl$:A (A = $Eu^{2+}$/$Ce^{3+}$/$Dy^{3+}$/$Tb^{3+}$) phosphors with multicolor emissions have been prepared as efficient phosphors for solid-state light and field-emission displays.

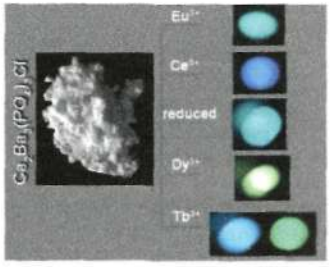


3113 dx.doi.org/10.1021/ic3025793

**Reactions of a Cyclodimethylsiloxane $(Me_2SiO)_6$ with Silver Salts of Weakly Coordinating Anions; Crystal Structures of $[Ag(Me_2SiO)_6][Al]$ ($[Al] = [FAl\{OC(CF_3)_3\}_3]$, $[Al\{OC(CF_3)_3\}_4]$) and Their Comparison with $[Ag(18\text{-Crown-}6)]_2[SbF_6]_2$**

T. Stanley Cameron, Andreas Decken, Ingo Krossing, Jack Passmore,* J. Mikko Rautiainen,* Xinping Wang, and Xiaoqing Zeng

Salts $[AgD_6][Al]$ ($[Al] = [Al\{OC(CF_3)_3\}_4]$, $[AlF\{OC(CF_3)_3\}_3]$) are the first examples of a preparation of transition metal ion host–guest complexes of cyclic dimethylsiloxanes directly from the components. Bonding and energetics of $[AgD_6]^+$ have been compared to analogous $[Ag(18\text{-crown-}6)]^+$ and other $[MD_n]^+$ (M = Ag, Li, $n$ = 4-8) complexes with theoretical calculations.

3127 dx.doi.org/10.1021/ic302583a

**Construction of a Polyhedral Metal–Organic Framework via a Flexible Octacarboxylate Ligand for Gas Adsorption and Separation**

Zu-Jin Lin, Yuan-Biao Huang, Tian-Fu Liu, Xiang-Ying Li, and Rong Cao*

A flexible octacarboxylate ligand, tetrakis[(3,5-dicarboxyphenyl)oxamethyl]methane ($H_8X$), has been used to construct a porous metal–organic framework, which is comprised of octahedral and cuboctahedral cages and shows a rare (4,8)-connected scu topology. Gas adsorption measurements and ideal adsorbed solution theory (IAST) calculations demonstrate that the framework has high selectivites of $CO_2$ over $CH_4$ and $N_2$. Remarkably, the resulting material represents a MOF with the highest gas uptakes and gas selectivities ($CO_2$ from $CH_4$ and $N_2$) constructed by the flexible ligand.

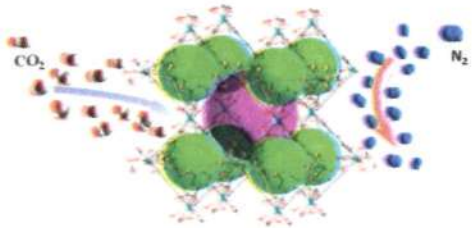


3133 dx.doi.org/10.1021/ic3026057

**Methylenediphosphonotetrathioate: Synthesis, Characterization, and Chemical Properties**

Aviran Amir, Alon Haim Sayer, Alon Ezra, and Bilha Fischer*

MDPT forms water-soluble complexes preferably with soft/borderline metal-ions. For instance, MDPT showed a 10,000,000-fold preference to Zn(II) vs Ca(II) ions.

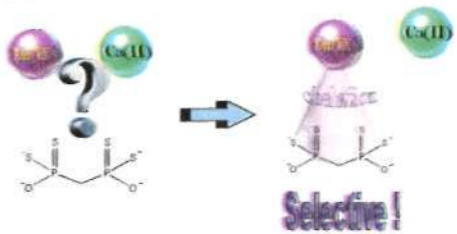


3141 dx.doi.org/10.1021/ic302608g

**Facile Synthesis of Graphene/Metal Nanoparticle Composites via Self-Catalysis Reduction at Room Temperature**

Qiqi Zhuo, Yanyun Ma, Jing Gao, Pingping Zhang, Yujian Xia, Yiming Tian, Xiuxiao Sun, Jun Zhong, and Xuhui Sun*

Facile synthesis of a graphene/metal NP composite with good control of size and morphology has been developed. The approach has been demonstrated to successfully synthesize graphene composites with various metal NPs in large quantity, which opens up a novel and simple way to prepare large-scale graphene/metal or graphene/metal oxide composites under mild conditions for practical applications. For example, graphene/AuNP composites synthesized by the method show excellent performance in the catalysis applications.

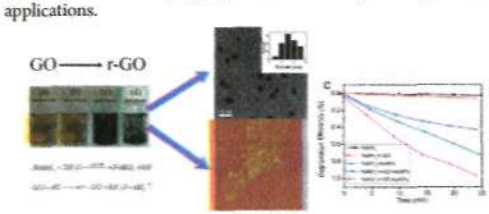




3148 dx.doi.org/10.1021/ic302627n

**Quaternary Arsenides $AM_{1.5}Tt_{0.5}As_2$ ($A$ = Na, K, Rb; $M$ = Zn, Cd; $Tt$ = Si, Ge, Sn): Size Effects in $CaAl_2Si_2$- and $ThCr_2Si_2$-Type Structures**

Mansura Khatun, Stanislav S. Stoyko, and Arthur Mar*

The quaternary arsenides $AM_{1.5}Tt_{0.5}As_2$ adopt either $CaAl_2Si_2$- or $ThCr_2Si_2$-type structures depending on the relative sizes of the $A$, $M$, and $Tt$ components, as can be represented on a structure map.

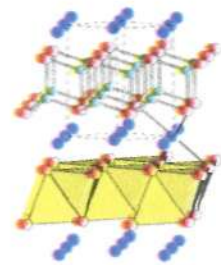

3159 dx.doi.org/10.1021/ic302634q

**Iron in a Trigonal Tris(alkoxide) Ligand Environment**

Matthew B. Chambers, Stanislav Groysman, Dino Villagrán, and Daniel G. Nocera*

Mononuclear compounds of $Fe^{2+}$ and $Fe^{3+}$ supported by tris(alkoxide) ligand scaffolds, $^tBu_3MeCO^-$ (ditox), have been synthesized and characterized. Whereas tris(ditox) complexes of trivalent iron where observed to be inert toward oxygen atom transfer reagents, divalent iron tris(ditox) species were found to react readily to transiently generate high valent intermediates. Subsequent observation of facile reactivity (HAT and oxo transfer) is attributed to the weakly donating tris(alkoxide) ligand field, which is calculated to stabilize high spin states.

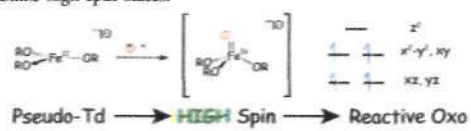


3170 dx.doi.org/10.1021/ic3026396

**Effects of Imidazole Deprotonation on Vibrational Spectra of High-Spin Iron(II) Porphyrinates**

Chuanjiang Hu,* Qian Peng, Nathan J. Silvernail, Alexander Barabanschikov, Jiyong Zhao, E. Ercan Alp, Wolfgang Sturhahn, J. Timothy Sage,* and W. Robert Scheidt*

The iron vibrations in the five-coordinate high-spin iron(II) porphyrinates with imidazole and imidazolate as the axila ligands are compared. The in-plane frequencies shift to lower frequency in the imdidazolate complexes, whereas the out-of-plane modes shift to higher frequency.

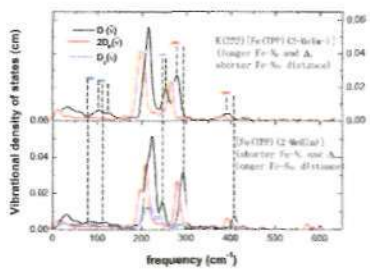

3178 S dx.doi.org/10.1021/ic302650r

**The Modulated Structure of $Co_3Al_4Si_2$: Incommensurability and Co−Co Interactions in Search of Filled Octadecets**

Rie T. Fredrickson and Daniel C. Fredrickson*

The origins of incommensurate modulations are often mysterious, but appear to be as diverse as the compounds in which they arise. We describe the crystal structure and bonding of $Co_3Al_4Si_2$ whose modulated structure can be traced to a central concept of inorganic chemistry: the 18 electron rule. Key to this compound's bonding are covalently shared electron pairs in orbitals isolobal to classical Co−Co $\sigma$ and $\pi$ bonds, but delocalized over bridging Si/Al atoms.

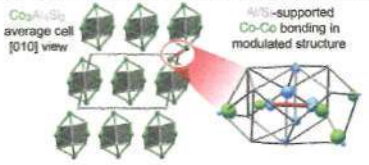


3190 S dx.doi.org/10.1021/ic302663c

**Improving the Efficiency of the Photoinduced Charge-Separation Process in a Rhenium(I)−Zinc Porphyrin Dyad by Simple Chemical Functionalization**

*Teresa Gatti, Paolo Cavigli, Ennio Zangrando, Elisabetta Iengo,* Claudio Chiorboli, and Maria Teresa Indelli**

The dyad system for efficient photoinduced electron transfer is given.

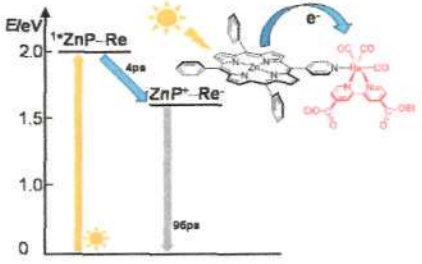


3198 S dx.doi.org/10.1021/ic302693n

**Synthesis, Structure, and Properties of $Ln_2Ru_3Al_{15}$ (Ln = Ce, Gd): Comparison with $LnRu_2Al_{10}$ and $CeRu_4(Al,Si)_{15.58}$**

*Gregory Morrison, Neel Haldolaarachchige, Chih-Wei Chen, David P. Young, Emilia Morosan, and Julia Y. Chan**

$Ln_2Ru_3Al_{15}$ (Ln = Ce, Gd) have been synthesized, and the competition between the growth of $Ce_2Ru_3Al_{15}$ and $CeRu_2Al_{10}$ has been studied. The structure of $Ce_2Ru_3Al_{15}$ was modified from the previously reported $Ce_2Ru_3Al_{15}$ structure, and the structure of $Gd_2Ru_3Al_{15}$ was determined for the first time. The magnetic and transport properties of $Ln_2Ru_3Al_{15}$ were measured and compared to the properties of $LnRu_2Al_{10}$.

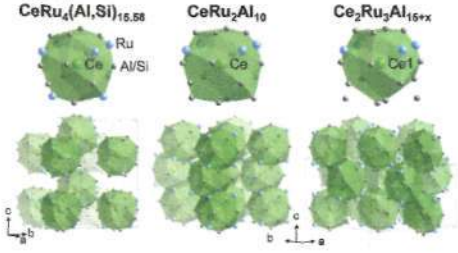




3207 S dx.doi.org/10.1021/ic302697v

**Nitric Oxide Release from a Nickel Nitrosyl Complex Induced by One-Electron Oxidation**

Ashley M. Wright, Homaira T. Zaman, Guang Wu, and Trevor W. Hayton*

Oxidation of $[Ni(NO)(bipy)][PF_6]$ with a variety of one-electron ($1e^-$) oxidants, including $AgPF_6$, $[NO][PF_6]$, and TEMPO, results in rapid release of NO gas. In the TEMPO reaction, the Ni-containing byproduct, $[(bipy)Ni(\eta^2\text{-TEMPO})][PF_6]$, can be isolated in good yield.

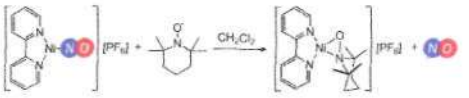


3217 S dx.doi.org/10.1021/ic302696m

**Solid-State and Solution-State Coordination Chemistry of Lanthanide(III) Complexes with (Pyrazol-1-yl)acetic Acid**

Xiao-Yan Chen,* George S. Goff,* Brian L. Scott, Michael T. Janicke, and Wolfgang Runde

As a precursor of carboxyl-functionalized task-specific ionic liquids (TSILs) for f-element separation, (pyrazol-1-yl)acetic acid (**L**) can be deprotonated as a functionalized pyrazolate anion to coordinate with hard metal cations. However, the coordination chemistry of **L** with f-elements remains unexplored. We reacted **L** with lanthanides in aqueous solution at pH = 5 and synthesized four lanthanide complexes of general formula $[Ln(L)_3(H_2O)_2]\cdot nH_2O$.

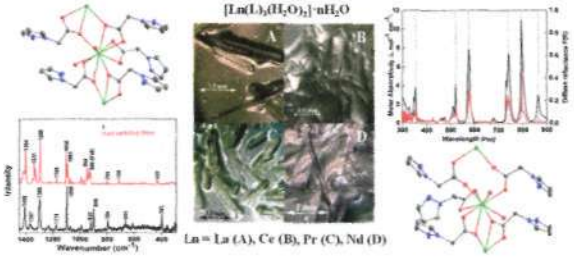


3225 S dx.doi.org/10.1021/ic302716

***Cd(II)*-Coordination Framework: Synthesis, Anion-Induced Structural Transformation, Anion-Responsive Luminescence, and Anion Separation**

Shan Hou, Qi-Kui Liu, Jian-Ping Ma, and Yu-Bin Dong*

A series of *Cd(II)*-coordination frameworks with anion-induced structural transformation, anion-responsive luminescence, and anion separation were reported.

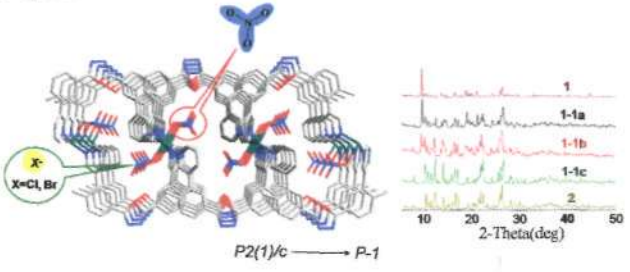

3236 dx.doi.org/10.1021/ic302735j

**By Design: A Macrocyclic 3d–4f Single-Molecule Magnet with Quantifiable Zero-Field Slow Relaxation of Magnetization**

Humphrey L. C. Feltham, Rodolphe Clérac, Liviu Ungur, Liviu F. Chibotaru, Annie K. Powell, and Sally Brooker*

$[Cu_3Tb(\mathbf{L}^{Bu_t})]$ is the first example of a macrocyclic 3d–4f single-molecule magnet that exhibits quantifiable relaxation of magnetization in zero dc field. Rational modification of the equatorially bound macrocycle tuned the ligand field and resulted in apical binding of *two* nitrate ions to the oblate Tb(III) ion, giving enhanced uniaxial anisotropy and SMM properties despite the low symmetry of the Tb(III) site.

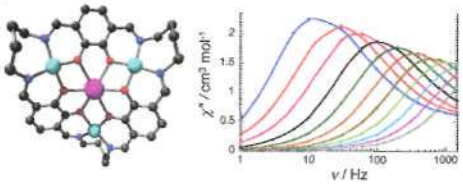


3241 dx.doi.org/10.1021/ic3027557

**Electrochemical and Spectroscopic Investigation of $Ln^{3+}$ (Ln = Sm, Eu, and Yb) Solvation in Bis(trifluoromethylsulfonyl) imide-Based Ionic Liquids and Coordination by *N,N,N′,N′*-Tetraoctyl-3-oxa-pentane Diamide (TODGA) and Chloride**

Yunfeng Pan and Charles L. Hussey*

Lanthanide ions can be introduced into bis(trifluoromethylsulfonyl)imide-based ionic liquids by anodic oxidation of the respective metals; $Eu^{3+}$, $Eu^{2+}$, $Sm^{3+}$, $Yb^{3+}$, and $Yb^{2+}$ but not $Sm^{2+}$ exhibit considerable stability. This article reports the electrochemistry and electronic absorption spectroscopy of these lanthanide ions in the neat ionic liquids and in these ionic solvents containing the neutral tridentate ligand *N,N,N′,N′*-tetra(*n*-octyl)diglycolamide (TODGA) and the anionic hard ligand chloride.

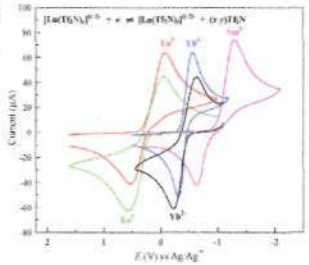

3253 dx.doi.org/10.1021/ic3027682

**$(C_4N_2H_{12})_3[Ln_3(OH)(SO_4)_7]$ (Ln = Sm, Eu, and Tb): A Series of Honeycomb-like Open-Framework Lanthanide Sulfates with Extra-Large Channels Containing 24-Membered Rings**

Deng Zhang, Yun Lu, Dunru Zhu, and Yan Xu*

Three novel honeycomb-like lanthanide sulfates with extra-large channels containing 24MR have been synthesized by using chair form piperazine as the structure-directing agent under one-pot solvothermal reactions. They are isostructural, and the open framework is the first lanthanide sulfate with extra-large channels containing 24MR. It has an ***acs*** framework topology.

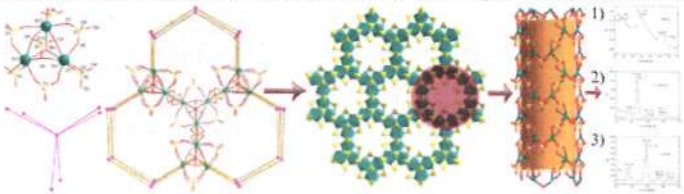




3259 dx.doi.org/10.1021/ic302771f

**Photo-initiated Thiol-ene Click Reactions as a Potential Strategy for Incorporation of $[M^I(CO)_3]^+$ (M = Re, $^{99m}$Tc) Complexes**

Thomas R. Hayes, Patrice A. Lyon, Elsa Silva-Lopez, Brendan Twamley, and Paul D. Benny*

The radical initiated thiol-ene click reaction between a thiol and an alkene was investigated for potential in $Re/^{99m}Tc^I(CO)_3$ radiopharmaceuticals applications by functionalizing a 2,2′-dipicolylamine chelate with an allyl group. Two strategies, *chelate then click* and *click then chelate*, were examined to determine the versatility of this click reaction in the presence of the metal, where both approaches were found to be capable of the thiol-ene click reaction at the macroscopic and tracer concentrations.

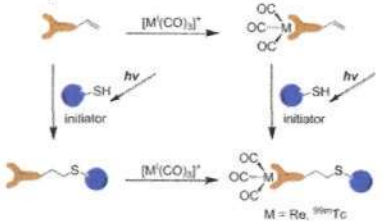


3268 dx.doi.org/10.1021/ic302785m

**$^1$H and $^{17}$O NMR Relaxometric and Computational Study on Macrocyclic Mn(II) Complexes**

Gabriele A. Rolla, Carlos Platas-Iglesias, Mauro Botta,* Lorenzo Tei, and Lothar Helm

The solution structure of Mn(II) complexes with a homogeneous series of chelators based on cyclen with one, two, and three acetic pendant arms was investigated by $^1$H and $^{17}$O NMR relaxometry and DFT calculations. Particular attention was devoted to the detailed study of the dynamics of the metal coordinated water molecule. Remarkably, [Mn(1,4-DO2A)] and [Mn(1,7-DO2A)] were found to be in equilibrium between the mono- and the nonhydrated species.

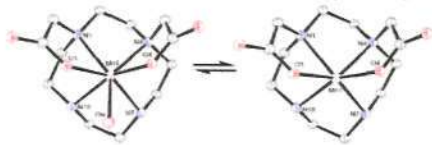

3280 dx.doi.org/10.1021/ic302788w

**Antimonato Polyoxovanadate Based Three-Dimensional Framework Exhibiting Ferromagnetic Exchange Interactions: Synthesis, Structural Characterization, and Magnetic Investigation of $\{[Fe(C_6H_{14}N_2)_2]_3[V_{15}Sb_6O_{42}(H_2O)]\}\cdot 8H_2O$**

Adam Wutkowski, Christian Näther, Paul Kögerler, and W. Bensch*

The spherical $[V_{15}Sb_6O_{42}]^{6-}$ cluster shell is bound to six $Fe^{2+}$-centered complexes, which join the clusters to form a three-dimensional network. Ferromagnetic exchange interactions are observed upon cooling.

3349 S dx.doi.org/10.1021/ic3028447

**Relationship between the Electron Density of the Heme Fe Atom and the Vibrational Frequencies of the Fe-Bound Carbon Monoxide in Myoglobin**

Ryu Nishimura, Tomokazu Shibata, Hulin Tai, Izumi Ishigami, Takashi Ogura,* Satoshi Nagao, Takashi Matsuo, Shun Hirota, Kiyohiro Imai, Saburo Neya, Akihiro Suzuki, and Yasuhiko Yamamoto*

We analyzed the vibrational frequencies of the Fe-bound carbon monoxide (CO) of myoglobin reconstituted with a series of chemically modified heme cofactors possessing a heme Fe atom with a variety of electron densities. The stretching frequency of Fe-bound CO ($\nu_{CO}$) was found to increase with decreasing electron density of the heme Fe atom ($\rho_{Fe}$). This finding demonstrated that the $\nu_{CO}$ value can be used as a sensitive measure of the $\rho_{Fe}$ value and that the $\pi$ back-donation of the heme Fe atom to CO is affected by the heme $\pi$-system perturbation induced through peripheral side chain modifications.

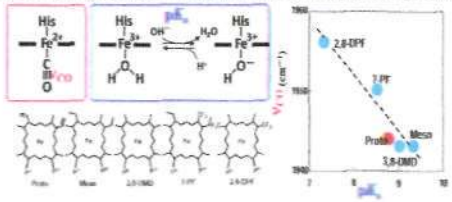


3356 S dx.doi.org/10.1021/ic302867y

**Geometric and Electronic Structures of Manganese-Substituted Iron Superoxide Dismutase**

Timothy A. Jackson, Craig T. Gutman, James Maliekal, Anne-Frances Miller, and Thomas C. Brunold*

The active-site structures of the oxidized and reduced forms of manganese-substituted iron superoxide dismutase (Mn(Fe)SOD) have been examined by employing a combination of spectroscopic and computational methods. Our spectroscopic data reveal that in its oxidized state, the active site of this species is virtually identical to that of wild-type manganese SOD (MnSOD), both featuring a trigonal bipyramidal ligand environment. This proposal is corroborated by quantum and molecular mechanical computations performed on complete protein models of Mn(Fe)SOD and MnSOD in both their oxidized and their reduced states.

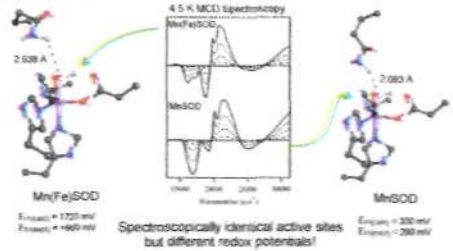




3368 S dx.doi.org/10.1021/ic400049k

**Gd–Sc-Based Mixed-Metal Nitride Cluster Fullerenes: Mutual Influence of the Cage and Cluster Size and the Role of Scandium in the Electronic Structure**

Anna L. Svitova, Alexey A. Popov,* and Lothar Dunsch*

The sythesis of mixed-metal nitride cluster fullerenes $Gd_xSc_{3-x}N@C_{2n}$ ($2n$ = 78–88) with melamine as the source of nitrogen is systematically studied, and the optimum cluster size for each carbon cage ranging from $C_{78}$ to $C_{88}$ is revealed. Spectroscopic, electrochemical, and density functional theory computational studies reveal the special role of scandium in $Gd_xSc_{3-x}N@C_{2n}$ molecules that affects the nature and energies of the frontier molecular orbitals.

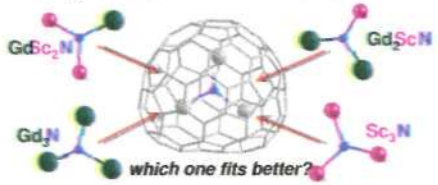


3381 S dx.doi.org/10.1021/ic4000473

**Cobalt Corrole Catalyst for Efficient Hydrogen Evolution Reaction from $H_2O$ under Ambient Conditions: Reactivity, Spectroscopy, and Density Functional Theory Calculations**

Biswajit Mondal, Kushal Sengupta, Atanu Rana, Atif Mahammed, Mark Botoshansky, Somdatta Ghosh Dey,* Zeev Gross,* and Abhishek Dey*

We report here an electronically tuned Co(III) corrole that can catalyze the HER from aqueous sulfuric acid at as low as −0.3 V vs NHE, with a turnover frequency of 600 $s^{-1}$ and $\gg 10^7$ catalytic turnovers. Under aerobic conditions, using $H_2O$ from naturally available sources without any pretreatment, the same complex catalyzes the reduction of both $O_2$ and $H^+$, utilizing the Co(II) and Co(I) oxidation states, respectively. The mechanism of the HER has been investigated with in situ spectroscopy and DFT.

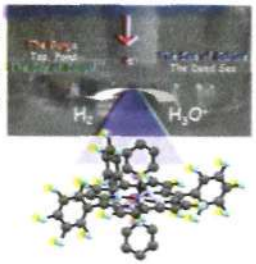


3388 S dx.doi.org/10.1021/ic400125x

**Topochemical Fluorination of $Sr_3(M_{0.5}Ru_{0.5})_2O_7$ (M = Ti, Mn, Fe), $n$ = 2, Ruddlesden–Popper Phases**

Fabio Denis Romero, Paul A. Bingham, Susan D. Forder, and Michael A. Hayward*

Reaction of the appropriate $Sr_3(M_{0.5}Ru_{0.5})_2O_7$ (M = Ti, Mn, Fe), $n$ = 2, Ruddlesden–Popper oxide with $CuF_2$ under flowing oxygen results in formation of the oxide–fluoride phases $Sr_3(Ti_{0.5}Ru_{0.5})_2O_7F_2$, $Sr_3(Mn_{0.5}Ru_{0.5})_2O_7F_2$, and $Sr_3(Fe_{0.5}Ru_{0.5})_2O_{5.5}F_{3.5}$ via a topochemical anion insertion/substitution process. Analysis indicates the titanium and manganese phases have $Ti^{4+}$, $Ru^{6+}$ and $Mn^{4+}$, $Ru^{6+}$ oxidation state combinations respectively, while Mössbauer spectra indicate an $Fe^{3+}$, $Ru^{5.5+}$ combination for the iron phase.

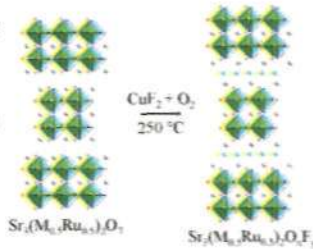

# Additions and Corrections



● Supporting Information available via online article